Orbital Selective Directional Conductor in the Two Orbital Hubbard Model

Anamitra Mukherjee[1,3], Niravkumar D. Patel[1], Adriana Moreo[1,2], and Elbio Dagotto[1,2]
[1] *Department of Physics and Astronomy, The University of Tennessee, Knoxville, Tennessee 37996, USA*
[2] *Materials Science and Technology Division, Oak Ridge National Laboratory, Oak Ridge, Tennessee 37831, USA and*
[3] *School of Physical Sciences, National Institute of Science Education and Research, Jatni 752050, India*

Employing a recently developed many-body technique that allows for the incorporation of thermal effects, the rich phase diagram of a two dimensional two orbital (degenerate d_{xz} and d_{yz}) Hubbard model is presented varying temperature and the repulsion U. Our main result is the finding at intermediate U of a novel antiferromagnetic orbital selective state where an effective dimensional reduction renders one direction insulating and the other metallic. Possible realizations of this state are discussed. In addition we also study nematicity above the Néel temperature. After a careful finite-size scaling analysis the nematicity temperature window appears to survive in the bulk limit although it is very narrow.

arXiv:1510.04902v2 [cond-mat.str-el] 10 Feb 2016

I. INTRODUCTION

Several important materials, such as iron-based high critical temperature superconductors (FeSC),[1–4] nickelates,[5] cobaltites,[6] manganites,[7,8] and many others, have several active orbitals. If electronic correlation effects are important, then multiorbital Hubbard models must be employed for their analysis. However, these models are difficult to study in two (2D) or three (3D) dimensions due to their complexity. While at particular electronic densities, such as integer fillings, zero temperature mean field (MF) approximations are often reliable, the phase diagrams of multiorbital Hubbard models varying *temperature* T are basically unknown. This is because thermal mean-field approximations provide qualitatively incorrect results at robust Hubbard repulsion U and intermediate temperature since they cannot generate local moments with short-range magnetic order because of the absence of spatial fluctuations. Moreover, "sign problems" complicate the application of quantum Monte Carlo (MC) when several orbitals are active.[9] Since not only U but also the Hund coupling J are important, it is imperative to apply alternative computational tools, even if crude, to study multiorbital models at intermediate temperatures because the potential for new states in these systems is considerable.

Recently,[10] the "Monte Carlo-Mean Field" (MC-MF) technique that mixes the MC and MF approximations was tested using the half-filled one-orbital Hubbard model. The method captured all qualitative features of this model known from quantum Monte Carlo, including the non-monotonic behavior of the Néel temperature T_N with increasing U, and it was even quantitatively accurate with errors of only $\sim$20% in T_N.[10] This method was applied before to the BEC-BCS crossover in the cold atom context and to other problems.[11] Early studies within the spin-fermion model context showed that this type of techniques are also reliable in studies of superconductors.[12–14]

The new method relies on the Hubbard-Stratonovich decomposition of the interacting problem via auxiliary fields (AuxF)[11–14] (in the Hartree channel in our study, but could be in other channels as well). Neglecting the AuxF's imaginary-time dependence but retaining their spatial fluctuations leads to a Hamiltonian with quantum fermions coupled to classical degrees of freedom, similarly as in double-exchange models for manganites.[7] Classical Monte Carlo is used for the AuxF at any temperature, while the fermionic sector is treated via the traveling cluster approximation (TCA) that allows access to large lattices.[15,16]

In this publication, the MC-MF technique is applied for the first time to a 2D two-orbital Hubbard model, varying temperature T and repulsion U. The unveiled phase diagram is rich, including a narrow nematic phase above T_N.[17,18] Even more importantly, here we report an unexpected novel regime, dubbed Orbital Selective Directional Conductor (OSDC), where a remarkable anisotropy in transport is observed, with one direction insulating and the other conducting, leading to a dimensional reduction from 2D to 1D. This dimensional reduction is different from that in $Tl_2Ru_2O_7$ and $BaCuSi_2O_6$ because they are insulating in all directions,[19,20] and different from layered $Sr_3Ru_2O_7$ because it requires a high magnetic field.[21] Our results are also different from layered oxides that are metallic in-plane but insulating out-of-plane,[22] because their crystal structure already establishes an asymmetry. On the contrary, our two-dimensional model is fully symmetric between the x and y directions but *spontaneously* becomes insulating in one direction and metallic in the other, without the help of the lattice, magnetic fields, or impurities.

II. MODEL AND METHOD

Although five orbitals are needed for a faithful electronic description of iron superconductors, below for simplicity we will focus on the two most important orbitals d_{xz} and d_{yz}.[23–26] The two-orbital Hubbard model studied here is defined as:

$$H = \sum_{\langle i,j\rangle,\alpha,\beta,\sigma} T^{i,j}_{\alpha,\beta} d^{\dagger}_{i,\alpha,\sigma} d_{j,\beta,\sigma} + U \sum_{i,\alpha} n_{i,\alpha,\uparrow} n_{i,\alpha,\downarrow} + (U' - J/2) \sum_{i} n_{i,xz} n_{i,yz} - 2J \sum_{i} S^{z}_{i,xz} S^{z}_{i,yz} + J' \sum_{i} (d^{\dagger}_{i,xz,\uparrow} d^{\dagger}_{i,xz,\downarrow} d_{i,yz,\downarrow} d_{i,yz,\uparrow} + H.c.), \quad (1)$$

where $d^{\dagger}_{i,\alpha,\sigma}$ creates an electron at site i, orbital α (either xz or yz), and with spin projection σ. The number operator is $n_{i,\alpha,\sigma}$, $n_{i,\alpha}$=$\sum_{\sigma} n_{i,\alpha,\sigma}$, and $S^{z}_{i,\alpha} = (1/2)(n_{i,\alpha,\uparrow} - n_{i,\alpha,\downarrow})$. U, U', J, and J' are the Kanamori parameters. The usual constraints $U' = U - 2J$ and $J = J'$ are assumed. In the Hund term only the Ising portion is used because the expected magnetic order is collinear, most materials have an easy-axis, and it is technically simpler for this first study. The hopping parameters reproduce the Fermi surface of the undoped FeSC,[23] but our conclusions could be realized as well in other materials with local tetragonal symmetry. The crystal location of the Se, As, or P atoms, used by electrons to tunnel from Fe to Fe, justify that both nearest- (NN) and next-nearest-neighbor (NNN) hoppings are needed. The explicit hopping amplitudes are in previous publications.[23,24] The NN sites hoppings t_1 and t_2 are only intraorbital. Along the plaquette diagonals, the intraorbital (interorbital) hopping is t_3 (t_4). Their values are t_1=1, t_2=−1.33, and t_3=t_4=−0.85 and the bandwidth of this tight binding model is W=12t_1.[23] Hereafter, t_1 will be denoted by t, and it will be the energy unit. To convert to eV, the *ab-initio* derived bandwidth for the d_{xz}-d_{yz} bands is $W \sim 1.8$ eV.[27,28] The density is fixed to two electrons per site ($n = 2$).

Mean-field approximations have already been applied to two-orbital Hubbard models at T=0,[25,26] showing several phases with increasing U/W: a paramagnetic metal, a metal with $(\pi, 0)$ spin order, and an insulator also with $(\pi, 0)$ spin order. These previous T=0 studies and others[1–4] showed that $J/U \sim 0.15-0.30$ is relevant for FeSC, and we will fix $J/U = 0.25$ in all the results below. Since FeSC materials vary substantially in their degree of electronic correlation, results will be presented varying the ratio U/W. Our main focus are the temperature effects since their influence on model Eq. (1) are unknown. Our study is performed in two dimensions, mainly on 32^2 lattices. The TCA traveling cluster[16] is 6^2. Via the parallelized version of TCA,[16] lattices as large as 48^2 were reached. The mean-field approach was chosen to be the Hartree approximation that works well for the half-filled one-orbital model.[29]

III. RESULTS

Our main results are in the phase diagram of model Eq.(1) at $n = 2$ (Fig. 1). It was constructed based on data for the two spin structure factors of relevance,

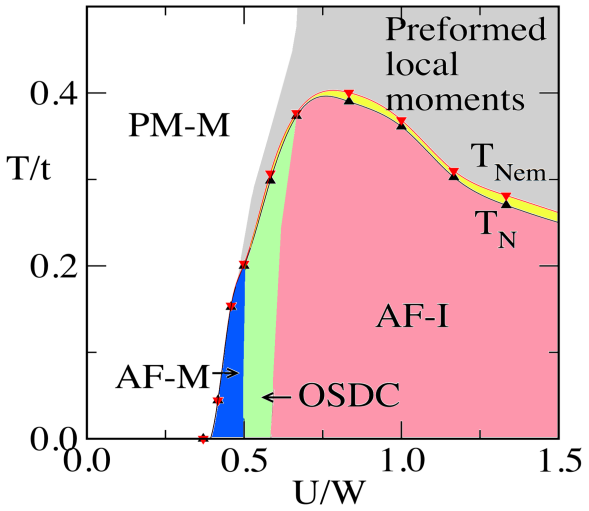

FIG. 1: (color online) Phase diagram of the two-orbital Hubbard model Eq.(1) in the MC-MF approximation and with hoppings from previous literature,[23] at $J/U = 0.25$ and $n = 2$. Shown are results for a 32^2 lattice. Besides the weak coupling paramagnetic metal (PM-M) and the intermediate/large U/W region with "preformed local moments" (grey), other states were identified: (1) A $(\pi, 0)$-spin-ordered metal, AF-M, where transport is anisotropic but metallic in both directions. (2) A novel $(\pi, 0)$-spin-ordered regime, the OSDC, with metallic (insulating) behavior along the x (y) axis. (3) A $(\pi, 0)$-spin-ordered insulator, AF-I, with a full gap. (4) A very narrow spin nematic regime above T_N. The AF-M and OSCD states break the same symmetries and, thus, no sharp distinction between them is expected but a rapid crossover. T_N has a non-monotonic behavior, maximizing close to the OSDC/AF-I boundary.

$S(\pi, 0)$ and $S(0, \pi)$, the spin nematic order parameter Ψ_{Nem},[18] their temperature derivatives, and the resistivity and density of states (DOS). We also monitored local moment formation at intermediate temperature and large U/W.[10] This phase diagram is surprisingly rich because it contains *three* regimes with $(\pi, 0)$ long-range magnetic order [degenerate with $(0, \pi)$]. The insulator at large U/W is induced by the robust J that produces S=1 local spins interacting via a frustrated Heisenberg model known to have $(\pi, 0)$-$(0, \pi)$ magnetic order. The other two states at intermediate couplings are more subtle. Intuitively, their magnetic order can be considered as arising from Fermi surface nesting effects. However, the presence of *two*, instead of one, regions is unexpected. The first one, dubbed AF-M (antiferromagnetic metallic), is metallic in both directions, albeit anisotropic, as observed in FeSC experiments.[17] But the second region, the OSDC, is metallic along the spin staggered direction but insulating along the spin uniform direction, leading to a surprising dimensional reduction at intermediate couplings.

A. Magnetic phases

A typical magnetic order parameter (OP) displays a negative curvature increasing temperature(Fig. 2a), with a diverging slope at the critical temperature T_c in the bulk limit. Thus, for a finite system the temperature where the first derivative $\mathrm{d}OP/\mathrm{d}T$ is maximized, or where the associated susceptibility maximizes, provides an estimation of T_c (here T_N and T_{Nem})(Fig. 2b). In addition, upon cooling T_{Nem} can also be estimated from the temperature T_{split} where $S(\pi,0)$ and $S(0,\pi)$ split. While for a finite system T_{Nem} and T_{split} may be different, they should merge in the bulk limit. Typical results are in Fig. 2 for a 32^2 lattice, at a fixed ratio U/W. Our MC statistics and lattice sizes are sufficient to observe a robust order parameter behavior for $S(\pi,0)$ and Ψ_{Nem}: nonzero at $T=0$ and decreasing with increasing temperature with a negative curvature, with the exception of a small temperature window where the curvature is positive due to size effects. Although very close in temperature, systematically for all the couplings U/W with long range spin order at $T=0$ and for all lattices, we find T_{Nem} slightly larger than T_N suggesting a small region of nematicity. In general, we also found that T_{split} tends to be larger than T_{Nem}. The observed narrow window of nematicity in fact appears to survive a finite-size scaling analysis (Fig. 3(a)), at least for the investigated coupling $U/W=1.16$ where information for lattices as large as 48^2 were gathered (since these simulations are very time consuming the scaling analysis could be done only for one coupling). Remarkably, within the error bars the bulk limit extrapolated T_{Nem} and T_{split} seem to lead to the same nematic critical temperature. More specifically, our results unveil a small nematic window of $\sim 0.002t$ at $U/W=1.16$. The narrowness of this nematic regime is likely exaggerated by the Z(2) nature of the Ising approximation used here for the Hund term. Such a fragile nematic phase, reported here for the first time in a Hubbard model, is compatible with previous studies using spin models,[30] spin-fermion models,[31] and with experiments,[17,32] that have also reported very narrow nematic temperature windows.

B. New State at Intermediate Coupling

As explained before it is surprising that there are three distinct regions below T_N: two metals (AF-M and OSDC) and one insulator (AF-I). The distinction between the two metals and the insulator can be understood via the density-of-states in Figs. 3(b,c). Panel (c) displays a canonical insulating behavior: in the temperature range shown, a pseudogap (PG) is observed in the local moments regime,[34] transforming into a full gap when the magnetic order develops at T_N. This is the AF-I state (Fig. 1). In panel (b), upon cooling toward T_N a pseudogap opens probably because of Fermi surface nesting effects. But even at low temperatures, and independently analyzing the zero-temperature Hartree equations, in both metallic regions the total DOS has a finite weight at the Fermi energy E_F.

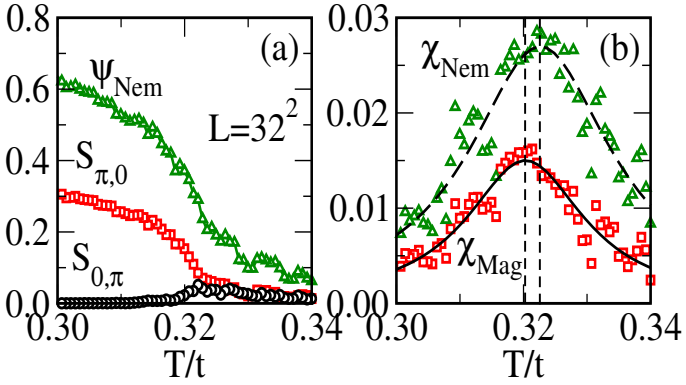

FIG. 2: (color online) (a) Spin structure factors and nematic order parameter at $U/W=1.16$ and using a 32^2 lattice (statistical errors bars are the size of the points; error bars due to trapping in metastable states are better represented by the fluctuations of the results with varying temperatures). (b) Same as (a) but for the magnetic(for $S(\pi,0)$ case) and nematic susceptibilities. Lorentzian fits of the data are shown. Vertical dashed lines (left to right) indicate the magnetic and nematic transition temperatures, from susceptibility maximization.

What is then the difference between AF-M and OSDC? Their physical distinction is illustrated in Fig. 4 (a) where the resistivity ρ vs. T is presented at three values of U/W, corresponding to the three low-temperature regions of Fig. 1. ρ is calculated from the optical conductivity $\sigma(\omega)$, integrating in a narrow range near $\omega=0$ and then inverting.[35] At $U/W=0.417$, ρ in the y spin uniform direction is larger than in the x spin staggered direction, as in previous calculations[31,36,37] and experiments.[17] This is understood from the orbital resolved DOS of Fig. 3(d): in the magnetic $(\pi,0)$ state that breaks rotational invariance, near E_F the orbital d_{yz}, related to conduction in the spin uniform direction, is more suppressed than d_{xz}, related to conduction in the spin staggered direction. But since both orbitals have a sizable DOS weight at the E_F, both directions are metallic. At large $U/W=1.0$, the DOS Fig. 3(c) displays a sharp gap at low temperature, and both directions must be insulating.

Note that experiments affected primarily by the vicinity of E_F may suggest strong orbital order, but the ω-integral of the orbital-resolved DOS, i.e. the orbital population n_{xz} and n_{yz}, is only different by 0.5% (Fig. 3 (f)).[33] For completeness, we also monitored $\Delta_{orb}=n_{xz}-n_{yz}$ vs. temperature. The results (not shown) indicate that upon cooling from high T, Δ_{orb} remains smaller than 0.001 at U/W=1.16 until T_{Nem} is reached, eventually converging, as T is further reduced, to the results derived from Fig. 3 (f). Within our MC accuracy we conclude that in our model there is no additional orbital-order critical temperature above T_{Nem}.

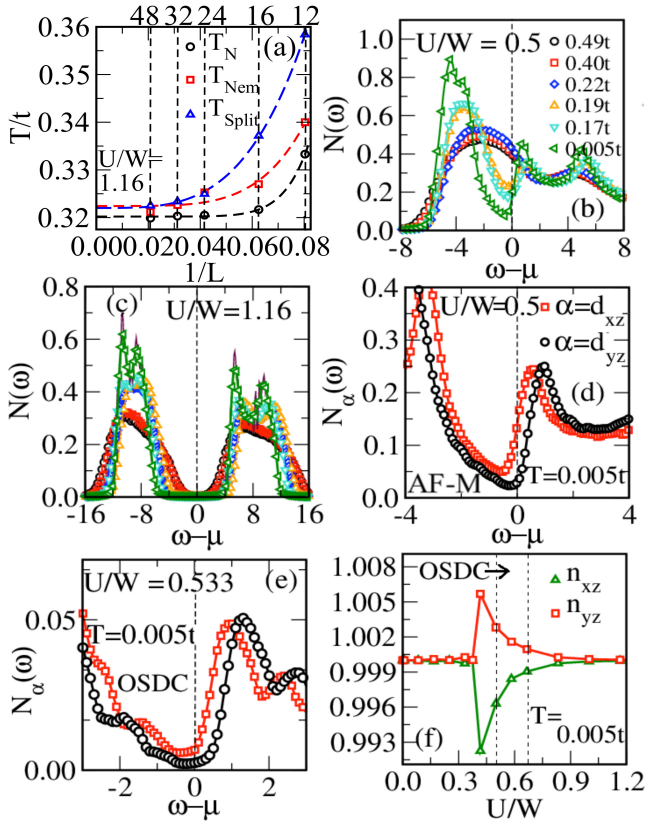

FIG. 3: (color online) (a) Finite-size scaling analysis for T_N, T_{Nem}, and T_{split} at $U/W = 1.16$, using $L = 12, ..., 48$ ($L \times L$) lattices plotted vs. $1/L$ (values at top). Data is fit with a scaling function $T_{ord}(L) = T_{ord}^{bulk} + b(1/L)^{(1/\nu)}$, where T_{ord}^{bulk}, b, and ν are independent fitting parameters for the three data sets. From the fit we obtain a nematic temperature window of width approximately $0.002t$. (b) Density of states $N(\omega)$ at U/W=0.5 (μ denotes E_F). A pseudogap develops below T_{Nem} that deepens with reducing temperature but never becomes a full gap. On the other hand, in panel (c) at U/W=1.16 a clear gap develops upon cooling. (d) contains the orbital-resolved DOS at T=0.005t and U/W=0.5. The C_4 spontaneous symmetry breaking makes the (nonzero) population of the two orbitals different at E_F.[33] (e) Same as (d), but at U/W=0.533 in the OSDC regime where $N_{yz}(\omega = \mu) << N_{xz}(\omega = \mu)$. (f) The orbital-resolved total occupation n_{xz} and n_{yz} shown at low T vs. U/W. Dashed lines indicate the OSDC regime. Panels (b-f) were obtained using 32^2 lattices.

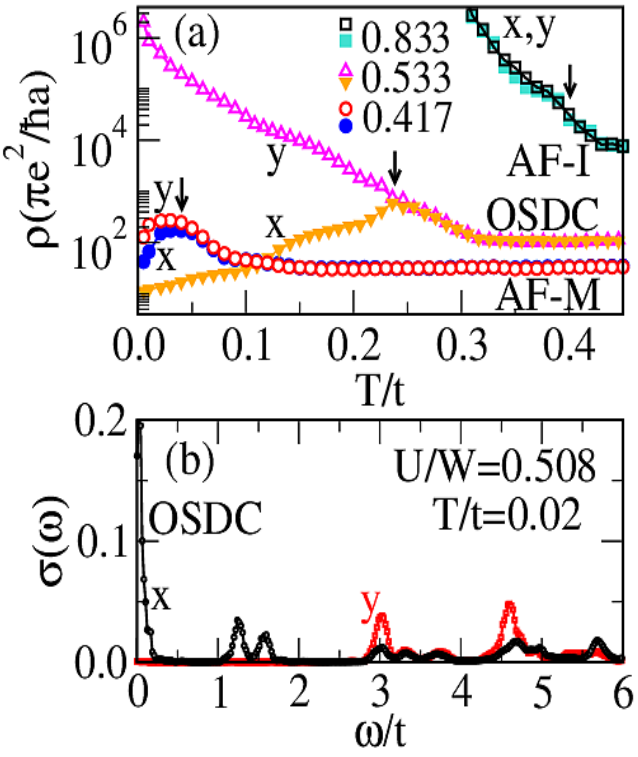

FIG. 4: (color online) (a) Resistivity along the x spin staggered (solid symbols) and y spin uniform (open symbols) directions at several U/W's, illustrating the transport properties of the AF-M, OSDC, and AF-I regions of Fig. 1. Arrows indicate T_N for each case. (b) Optical conductivity in the OSDC with electric fields along the y and x directions. In both panels a 16^2 lattice is used.

The interpolation between small and large U/W unveils a surprise: at intermediate couplings such as $U/W = 0.533$ the spin staggered direction remains metallic, but the spin uniform direction becomes *insulating* (Fig. 4 (a)). Intuitively, this is because the interpolation between the density-of-states of Fig. 3(d), where both orbitals have nonzero weight at E_F, and (c), where both orbitals have negligible weight at E_F, is not smooth. Instead, there is an intermediate coupling range where the d_{yz} weight at E_F is almost negligible while that of d_{xz} is still finite (Fig. 3(e)). The d_{yz} weight is very small but not zero, even at $T = 0$, because of the broadening used for density of states. Therefore, strictly speaking it cannot be used as a sharp order parameter: AF-M and OSDC are likely analytically connected because they break the same symmetries. However, our study shows that the orbital population difference at E_F in the OSDC is sufficiently large to induce one-dimensional transport. Results for the full $\sigma(\omega)$ (see Fig. 4 (b) and Appendix) show that at $\omega \sim 0$ only one orbital dominates. Moreover, from n_{xz} and n_{yz} (Fig. 3 (f)) note that at large U/W both orbital populations converge to one since J is large, while in the PM-M regime they are also one by symmetry. However, in the OSDC region *both* n_{xz} and n_{yz} are different from one (and different among themselves because C_4 is spontaneously broken): the OSDC regime is not the same as an Orbital Selective Mott Phase[38] where one orbital has population exactly one. Another interesting observation is that for both AF-M and OSDC there is an insulating region $d\rho/dT < 0$ in both directions immediately above T_N due to the opening of the pseudogap in the local moments region and concomitant coexisting patches of (π,0) and (0,π) order,[37] in agreement with spin fermion studies[37] and experiments.[17]

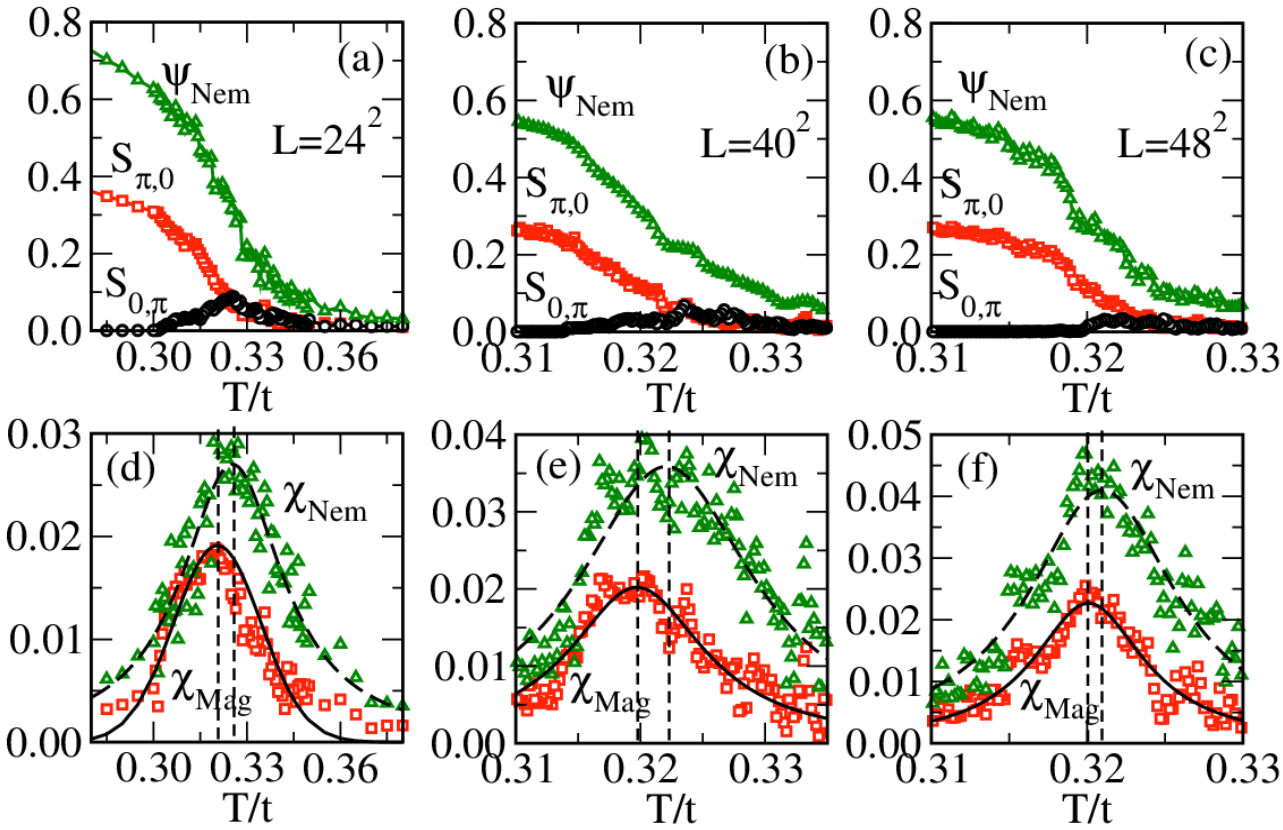

FIG. 5: (color online) (a,b,c) The $(\pi, 0)$ and $(0, \pi)$ magnetic structure factors, and the nematic order parameter (Ψ_{Nem}) vs. temperature for different lattice sizes, at $U/W = 1.16$. (d,e,f) Magnetic and nematic susceptibilities at $U/W = 1.16$ for the same lattice sizes as immediately above (i.e. (d) corresponds to (a), etc). The solid curves are Lorentzian fits. The dashed lines indicate the positions of the maxima in the susceptibilities, therefore indicating the estimated critical temperatures.

C. Other results used to construct the magnetic phase diagram

The analysis presented in Fig. 2 and Fig. 3(a) are just examples of the vast computational study carried out at various values of U/W and used to construct the phase diagram of Fig. 1. For completeness, in Fig. 5 this substantial effort is illustrated further by providing data corresponding to other lattice sizes at $U/W = 1.16$. The information gathered from these efforts for T_N, T_{Nem}, and T_{split} were used for the finite-size scaling analysis of Fig. 3 (a).

IV. CONCLUSIONS

The phase diagram of a layered two-orbitals Hubbard model was studied with emphasis on temperature effects. We report a novel intermediate coupling U region, called the OSDC, that is conducting in one direction via the d_{xz} orbitals, but insulating in the other because the associated d_{yz} orbitals have nearly vanishing weight at E_F. Although our low temperature calculations do not include quantum fluctuations, the OSDC starts at relatively high temperatures $\sim T_N$ and for this reason our approach emphasizing thermal effects should be sufficient. Moreover, we tested that using other hoppings,[39] the OSDC is also found. Experimentally, materials of the family of iron superconductors are the most likely to realize the OSDC (in fact, indications of OSDC are already present in Ref. 17 for the case of doped materials), and a mixing in the chemical formula of As, associated with weak coupling, and Se, associated with strong coupling, may be needed. But the OSDC could be realized in other layered materials where a transition metal atom M is coordinated with four ligand atoms X, establishing MX_4 tetrahedral cages with near degenerate d_{xz} and d_{yz} orbitals, and where a magnetic state that breaks lattice rotational invariance

is stabilized.

V. ACKNOWLEDGMENTS

E. Dagotto thanks Guangkun Liu for useful conversations. A. Mukherjee and N. Patel were supported by the National Science Foundation Grant No. DMR-1404375. E. Dagotto and A. Moreo were supported by the U.S. Department of Energy, Office of Basic Energy Science, Materials Science and Engineering Division.

VI. APPENDIX

A. Details of the Monte Carlo simulation and observables measured

The lattices used all have periodic boundary conditions. In our calculations, a total of 4000 MC system sweeps were typically performed: 2000 to thermalize the system, and the rest for calculating observables. A MC system sweep consists of sequentially visiting every lattice site and updating the local auxiliary fields followed by the fermionic diagonalization or TCA procedure to accept/reject via the Metropolis algorithm. We start the simulation at high temperature with a random configuration of auxiliary fields and then slowly cool down to lower temperatures to avoid being trapped in metastable states. The MC runs start at $T = 1.0t$, which corresponds to about 1000 K and cool down to $T = 0.005t$, where temperature steps as small as $\Delta T = 0.0002t$ were used for the temperatures relevant to the magnetic and nematic transitions. This slow process allows us to obtain reliable results independent of the initial conditions of the calculation.

In our finite systems, there is no energy difference between the $(\pi, 0)$ and $(0, \pi)$ magnetic states. As a consequence, MC simulations that start at high temperature in a random state for the auxiliary fields may end up in $(\pi, 0)$ or $(0, \pi)$ with equal chance upon cooling. In practice, we simply discarded all cooling down MC processes that led to a $(0, \pi)$ state at low temperatures.

The antiferromagnetic order is studied via the spin structure factors,

$$S(\mathbf{q}) = \frac{1}{L^4} \sum_{i,j} e^{i\mathbf{q}\cdot(\mathbf{r}_i - \mathbf{r}_j)} \langle S_i^z S_j^z \rangle. \quad (2)$$

The two wavevectors of interest in FeSC are $\mathbf{q} = (\pi, 0)$ and $(0, \pi)$. The expectation value is generated by using the eigenvectors of the MC equilibrated configurations. For the study of the nematic regime above T_N, we compute the nematic order parameter

$$\Psi_{Nem} = \frac{1}{2L^2} \sum_{i,\pm} (S_i^z S_{i\pm\hat{y}}^z - S_i^z S_{i\pm\hat{x}}^z), \quad (3)$$

where $\hat{x}$ and $\hat{y}$ are unit vectors connecting site i with its nearest neighbors. The $\pm$ summation is over all nearest neighbors, and $\langle \Psi_{Nem} \rangle > 0$ in the $(\pi, 0)$ magnetic phase. To better locate critical temperatures, we also calculate numerically the magnetic (χ_S) and nematic (χ_{Nem}) susceptibilities using the standard variance calculation.

In this work, we have also evaluated the orbital resolved density of states (DOS), $N_\alpha(\omega) = \sum_m |\langle \xi_{m,\alpha} | \psi \rangle|^2 \delta(\omega - \omega_m)$, where ω_m are the eigenvalues of the fermionic sector and the summation runs up to $2L^2$, i.e. the total number of eigenvalues of a L^2 system with spin. $|\langle \xi_{m,\alpha} | \psi \rangle|^2$ is the weight of the m^{th} eigenstate for orbital α in the state $|\psi\rangle$. $N_\alpha(\omega)$ is calculated by implementing the usual Lorentzian representation of the δ function. The broadening needed to obtain $N(\omega)$ from the Lorentzian is $\sim W/2L^2$, where W is the fermionic bandwidth at $U = 0$. Finally, $N(\omega)$, the total DOS, is the sum of the different orbital densities of states. Numerically, e.g., for the 8^2 system the broadening is about $0.09t$. Two hundred $N_\alpha(\omega)$ samples are obtained from the 2000 measurement system sweeps at every temperature. We discard 10 MC steps between measurements to reduce self-correlations in the data. The 200 $N_\alpha(\omega)$ samples are used to obtain the thermally averaged $\langle N_\alpha(\omega) \rangle_T$ at a fixed temperature. These are further averaged over data obtained from 10 independent runs with different random number seeds. A very similar procedure is followed to calculate the optical conductivity, that involves matrix elements of the current operator.

To determine the crossover temperature between the weak coupling paramagnetic state and the regime with preformed local moments above the magnetic order, we compute the specific heat, $C_v(U, J, T) = \frac{dE(U,J,T)}{dT}$, by numerically differentiating the average energy with respect to temperature, as well as the orbital resolved double occupation $\langle n_{\alpha,\uparrow} n_{\alpha,\downarrow} \rangle$. The details of the procedure we followed is presented in our earlier work on the one-orbital Hubbard model,[10] but, briefly, $C_v(U, J, T)$ has a high-temperature peak that corresponds to local moment formation that can be tracked varying U. In addition, the double occupation has to be below a cutoff for the system to have local moments.[10] This is of particular importance at small U values because $C_v(U, J, T)$ can have a considerable contribution from the electronic delocalization and in this regime it cannot be used to track local moment formation.

B. Test of the Technique in the Hartree Approximation

The many-body technique used in this publication was already introduced and tested in previous efforts.[10] However, since an easy axis is present in most materials and considering that empirically the Monte Carlo convergence is improved under such circumstances (colloquially, Ising is easier than Heisenberg), in this project it was decided to use the Ising approximation in the Hund

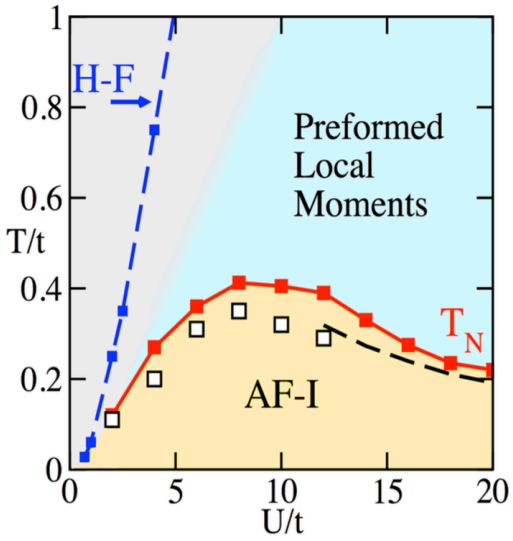

FIG. 6: (color online) The Hubbard U/t vs. temperature T/t phase diagram corresponding to the one-orbital Hubbard model in three dimensions using the Hartree approximation in the MC-MF technique. T_N denotes the Néel critical temperature where antiferromagnetism with (π, π, π) staggered magnetic order develops (region denoted as AF-I) according to measurements of the spin structure factor and the spin-spin correlation functions. The MC-MF results (red filled squares) are compared against data obtained using the Determinant Quantum Monte Carlo [white squares, reproduced from R. Staudt *et. al*, Eur. Phys. J. **B** 17, 411 (2000)]. The lattice size used in the MC-MF method is 4^3. The expected $4t^2/U$ behavior at large U/t is indicated by the black dashed line. The more crude mean-field Hartree Fock approximation results are denoted by "H-F" (blue dashed line): it incorrectly predicts the growth of the critical temperature with increasing U/t. In the light blue region measurements of the spin square operator and the double occupancy indicate the presence of a local moment.[10]

term. In the language of the one-orbital Hubbard model that corresponds to using the Hartree approximation instead of the Hartree-Fock approximation employed before. This requires, then, a test of the Hartree assumption for the three-dimensional one-orbital standard Hubbard model at half-filling. There is no need to provide explicitly the Hamiltonian for such well known model, thus we move immediately to discuss the results, which are provided in Fig. 6.

The results shown in Fig. 6 are encouraging. The critical temperatures found with the MC-MF technique capture the "up and down" behavior of T_N with increasing U/t and they converge close to the expected scaling at large U/t. Moreover, in the entire range of U/t investigated the MC-MF results are close to those of quantum Monte Carlo (with the largest discrepancy being about 20%). The successful test presented in Fig. 6 suggests that the MC-MF technique captures the essence of the one-orbital problem, not only qualitatively but also quantitatively. This gives us confidence that the results for two orbitals in the main text, that have not been studied before in the literature, are reliable.

C. Optical Conductivity

To illustrate the physics of the three different states reported here, the optical conductivity was calculated. The results are in Fig. 7. Panel (a) is in the AF-M regime: while the $(\pi, 0)$ magnetic order breaks the symmetry between the x and y directions, the difference is not dramatic and leads to both directions being metallic. Panel (c) corresponds to the Mott insulating regime: here a gap is present both when the electric field points along the x and y directions. The first excitations occur at the scale of the Hund coupling, along the x spin staggered direction. The most novel result is shown in panel (b), already presented in the main text and reproduced here for the benefit of the readers, corresponding to the new OSDC region: here at $\omega/t \sim 0$ there is a finite weight in the x direction but negligible weight in the y direction, compatible with the calculation of the resistivity shown in the main text.

Some subtle technical details are worth discussing, particularly with regards to the window in ω, around zero, used to define the resistivity. Consider a L^2 lattice. Its associated mean level spacing is roughly estimated as $s = W/(4L^2)$ where W is the bandwidth. In practice the individual δ-functions broadening used in the conductivity calculation is s times a factor, which it has been chosen to be 4 in our calculations. As example, for a 20^2 system $s = 12/(4 \times 20^2) = 0.0075$, and the broadening used is then 0.03. The integration range is decided as follows: the smallest frequency (the starting ω) is chosen to be at least one order of magnitude smaller than s. The frequency increment is chosen to be $s/10$. The data of these 10 frequency points is used for the integration and the outcome is ascribed as the average conductivity for the frequency value at the lower end of the interval. In the example given above, then the frequency step is 0.003. The integration is performed over 10 frequency steps. The calculation is started at an initial frequency of $0.0001t$.

D. Mean field formalism

For completeness, here details of the mean-field approximation are provided. In general, the multiorbital Hubbard model shown in the main text can be written as follows:

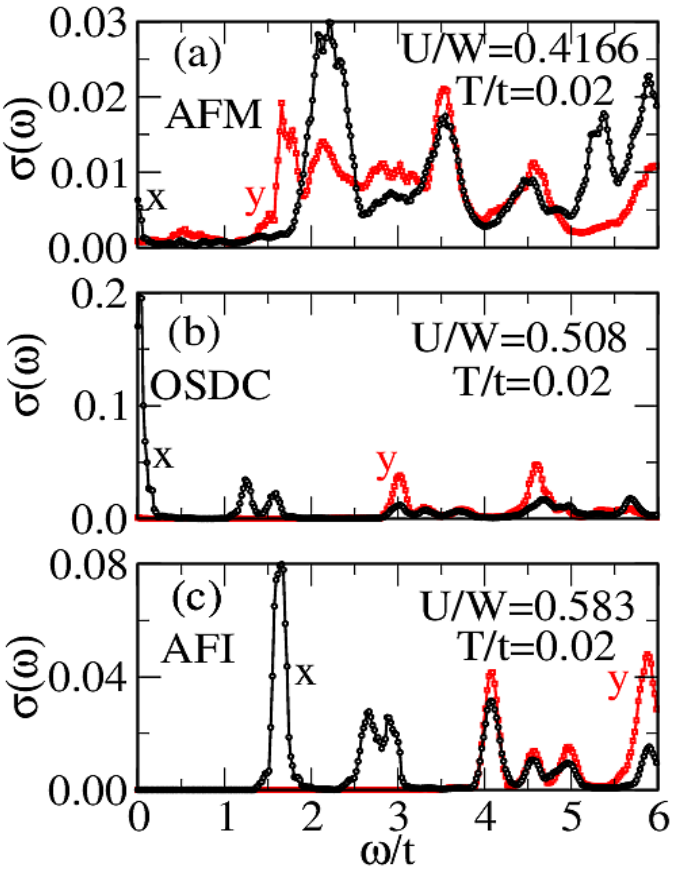

FIG. 7: (color online) Optical conductivity of the 2D two-orbital model used in this study at the temperatures and couplings U/W indicated. Panel (a) is in the AF-M regime; panel (b) in the OSDC regime; and panel (c) in the AF-I state. All data are using a 16^2 system.

$$H = H_o + H_{int} = \sum_{\langle i,j\rangle,\alpha,\beta,\sigma} T^{i,j}_{\alpha,\beta} d^\dagger_{i,\alpha,\sigma} d_{j,\beta,\sigma} + \sum_{i,\sigma,\sigma'} \sum_{\alpha,\alpha',\beta,\beta'} U_{\sigma,\sigma'}(\alpha,\alpha',\beta,\beta') d^\dagger_{i,\alpha,\sigma} d^\dagger_{i,\alpha',\sigma'} d_{i,\beta',\sigma'} d_{i,\beta,\sigma}. \quad (4)$$

H_o (H_{int}) in the kinetic (interaction) term. $d^\dagger_{i,\beta,\sigma}$ creates an electron at site i^{th}, orbital β, and with spin projection σ. The onsite interaction is:

$$\begin{aligned} U_{\sigma,\sigma'}(\alpha,\alpha',\beta,\beta') &= \frac{U}{2}\delta_{-\sigma,\sigma'}\delta_{\alpha,\alpha'}\delta_{\alpha\beta}\delta_{\alpha\beta'} \\ &+ \frac{U'}{2}(1-\delta_{\alpha\alpha'})\delta_{\alpha\beta}\delta_{\alpha'\beta'} \\ &+ \frac{J}{2}(1-\delta_{\alpha\alpha'})\delta_{\alpha\beta'}\delta_{\alpha'\beta} \\ &+ \frac{J'}{2}\delta_{\alpha\alpha'}\delta_{\beta\beta'}(1-\delta_{\sigma\sigma'})(1-\delta_{\alpha\beta}). \end{aligned} \quad (5)$$

To derive the MF Hamiltonian we follow the treatment in *Quantum Theory of Finite Systems*, by Blaizot, J.-P. & Ripka, G., The MIT Press (1985). The advantage of this approach is that one can derive a single general expression for the mean field parameters, for any number of orbitals. This expression can be easily coded in, thus avoiding the need to derive all possible mean field decouplings by hand. For this purpose we introduce the following notation:

$$\rho_{i,j,\alpha,\beta} = \langle\alpha|\rho_{i,j}|\beta\rangle = \langle d^\dagger_{j,\beta} d_{i,\alpha}\rangle, \quad (6)$$

where $\rho_{i,j,\alpha,\beta}$ are elements of the single particle density matrix. We now make the Hartree-Fock approximation assumption: the state of the system can be represented by a single Slater determinant, $|\Psi\rangle$. By using the Wick's theorem, we can then write down the expectation value of H in $|\Psi\rangle$, denoted by $E[\rho]$, as:

$$\begin{aligned} E[\rho] = &\sum_{\langle i,j\rangle,\alpha,\beta,\sigma} T^{i,j}_{\alpha,\beta}\langle\beta,\sigma|\rho_{i,j}|\alpha,\sigma\rangle + \\ &\sum_{i,\sigma,\sigma'}\sum_{\alpha,\alpha',\beta,\beta'} U_{\sigma,\sigma'}(\alpha,\alpha',\beta,\beta')\times \\ &[\langle\beta,\sigma|\rho_{i,i}|\alpha,\sigma\rangle\langle\beta',\sigma'|\rho_{i,i}|\alpha',\sigma'\rangle \\ &-\langle\beta',\sigma'|\rho_{i,i}|\alpha,\sigma\rangle\langle\beta,\sigma|\rho_{i,i}|\alpha',\sigma'\rangle]. \end{aligned} \quad (7)$$

We now take the derivative of $E[\rho]$ with respect to a generic density matrix element, $\langle\bar\alpha,\bar\sigma|\rho_{i,i}|\bar\beta,\bar\sigma'\rangle$, to get an explicit formula for Hartree-Fock mean field parameters, $\langle\bar\beta,\bar\sigma'|h|\bar\alpha,\bar\sigma\rangle$. Running over all values of orbitals and spin in $\langle\bar\alpha,\bar\sigma|\rho_{i,i}|\bar\beta,\bar\sigma'\rangle$, for taking the derivatives, generates all possible mean field decouplings in the Hartree-Fock channel. Thus, the general formula is as follows:

$$\begin{aligned} \langle\bar\beta,\bar\sigma'|h|\bar\alpha,\bar\sigma\rangle = &\sum_{\alpha',\beta'}(\sum_{\sigma'} \\ &[U_{\bar\sigma\sigma'}(\bar\beta,\alpha',\bar\alpha,\beta')\delta_{\bar\sigma\bar\sigma'} + U_{\sigma'\bar\sigma}(\alpha',\bar\beta,\beta',\bar\alpha)\delta_{\bar\sigma\bar\sigma'}]\times \\ &\langle\beta',\sigma'|\rho_{i,i}|\alpha',\sigma'\rangle \\ &-[U_{\bar\sigma'\bar\sigma}(\bar\beta,\alpha',\beta',\bar\alpha) + U_{\bar\sigma\bar\sigma'}(\alpha',\bar\beta,\bar\alpha,\beta')]\times \\ &\langle\beta',\bar\sigma'|\rho_{i,i}|\alpha',\bar\sigma\rangle). \end{aligned} \quad (8)$$

Finally, the full Hartree-Fock Hamiltonian is given by:

$$\begin{aligned} h_{MF} = &\sum_{\langle i,j\rangle,\alpha,\beta,\sigma} T^{i,j}_{\alpha,\beta} d^\dagger_{i,\alpha,\sigma} d_{j,\beta,\sigma} \\ &+ \sum_{i,\bar\alpha,\bar\sigma}\sum_{\bar\beta\bar\sigma'}\langle\bar\beta,\bar\sigma'|h|\bar\alpha,\bar\sigma\rangle d^\dagger_{i,\bar\alpha,\bar\sigma} d_{i,\bar\beta\bar\sigma'} \\ &- \sum_{i,\sigma,\sigma'}\sum_{\alpha,\alpha',\beta,\beta'} U_{\sigma,\sigma'}(\alpha,\alpha',\beta,\beta')\times \\ &(\langle\beta,\sigma|\rho_{i,i}|\alpha,\sigma\rangle\langle\beta',\sigma'|\rho_{i,i}|\alpha',\sigma'\rangle \\ &-\langle\beta',\sigma'|\rho_{i,i}|\alpha,\sigma\rangle\langle\beta,\sigma|\rho_{i,i}|\alpha',\sigma'\rangle). \end{aligned} \quad (9)$$

[1] D. C. Johnston, Adv. Phys. **59**, 803 (2010).
[2] P. J. Hirschfeld, M. M. Korshunov, and I. I. Mazin, Rep. Prog. Phys. **74**, 124508 (2011).
[3] P. Dai, J.-P. Hu, and E. Dagotto, Nat. Phys. **8**, 709 (2012).
[4] E. Dagotto, Rev. Mod. Phys. **85**, 849 (2013).
[5] J. B. Torrance, P. Lacorre, A. I. Nazzal, E. J. Ansaldo, and Ch. Niedermayer, Phys. Rev. B **45**, 8209(R) (1992).
[6] Y. Tokura, Y. Okimoto, S. Yamaguchi, H. Taniguchi, T. Kimura, and H. Takagi, Phys. Rev. B **58**, R1699(R) (1998).
[7] E. Dagotto, T. Hotta, and A. Moreo, Phys. Rep. **344**, 1 (2001).
[8] M. B. Salamon and M. Jaime, Rev. Mod. Phys. **73**, 583 (2001).
[9] For a recent reference see V. I. Iglovikov, E. Khatami, R. T. Scalettar, Phys. Rev. B **92**, 045110 (2015).
[10] A. Mukherjee, N. D. Patel, S. Dong, S. Johnston, A. Moreo, and E. Dagotto, Phys. Rev. B **90**, 205133 (2014).
[11] R. Tiwari and P. Majumdar, arXiv:1301.5026; R. Tiwari and P. Majumdar, arXiv:1302.2922; S. Tarat and P. Majumdar, Europhys. Lett. **105**, 67002 (2014); S. Tarat and P. Majumdar, arXiv:1402.0817; S. Tarat and P. Majumdar, arXiv:1406.5423.
[12] M. Mayr, G. Alvarez, C. Sen, and E. Dagotto, Phys. Rev. Lett. **94**, 217001 (2005).
[13] G. Alvarez, M. Mayr, A. Moreo, and E. Dagotto, Phys. Rev. **B 71**, 014514 (2005).
[14] M. Mayr, G. Alvarez, A. Moreo, and E. Dagotto, Phys. Rev. **B 73**, 014509 (2006).
[15] S. Kumar and P. Majumdar, Eur. Phys. J. **B 50**, 571 (2006).
[16] A. Mukherjee, N. D. Patel, C. Bishop, and E. Dagotto, Phys. Rev. E **91**, 063303 (2015).
[17] J-H. Chu, J. G. Analytis, K. De Greve, P. L. McMahon, Z. Islam, Y. Yamamoto, and I. R. Fisher, Science **329**, 824 (2010); I. R. Fisher, L. Degiorgi, and Z. X. Shen, Rep. Prog. Phys. **74**, 124506 (2011).
[18] R. M. Fernandes, A. V. Chubukov, and J. Schmalian, Nature Phys. **10**, 97 (2014); R. M. Fernandes, A. V. Chubukov, J. Knolle, I. Eremin, and J. Schmalian, Phys. Rev. B **85**, 024534 (2012); and references therein.
[19] S. Lee, J.-G. Park, D. T. Adroja, D. Khomskii, S. Streltsov, K. A. McEwen, H. Sakai, K. Yoshimura, V. I. Anisimov, D. Mori, R. Kanno, and R. Ibberson, Nat. Mater. **5**, 471 (2006).
[20] S. E. Sebastian, N. Harrison, C. D. Batista, L. Balicas, M. Jaime, P. A. Sharma, N. Kawashima, and I. R. Fisher, Nature **441**, 617 (2006).
[21] R. A. Borzi, S. A. Grigera, J. Farrell, R. S. Perry, S. J. S. Lister, S. L. Lee, D. A. Tennant, Y. Maeno, and A. P. Mackenzie, Science **315**, 214 (2007).
[22] H. M. Ronnow, Ch. Renner, G. Aeppli, T. Kimura, and Y. Tokura, Nature **440**, 1025 (2006); T. Valla, P. D. Johnson, Z. Yusof, B. Wells, Q. Li, S. M. Loureiro, R. J. Cava, M. Mikami, Y. Mori, M. Yoshimura, and T. Sasaki, Nature **417**, 627 (2002).
[23] S. Raghu, Xiao-Liang Qi, Chao-Xing Liu, D. J. Scalapino, and S.-C. Zhang, Phys. Rev. **B 77**, 220503 (2008).
[24] A. Moreo, M. Daghofer, J. A. Riera, and E. Dagotto, Phys. Rev. B **79**, 134502 (2009).
[25] Q. Luo, D.-X. Yao, A. Moreo, and E. Dagotto, Phys. Rev. B **83**, 174513 (2011).
[26] A. Nicholson, W. Ge, X. Zhang, J. Riera, M. Daghofer, A. M. Oleś, G. B. Martins, A. Moreo, and E. Dagotto, Phys. Rev. Lett. **106**, 217002 (2011); A. Nicholson, W. Ge, J. Riera, M. Daghofer, A. Moreo, and E. Dagotto, Phys. Rev. **B 85**, 024532 (2012).
[27] O.K. Andersen and L. Boeri, Annalen der Physik **523**, Issue 1-2, (2011).
[28] Note that the actual bandwidth is likely to be smaller as a result of a significant mass renormalization in the undoped FeSC materials.
[29] In the Hartree approximation the J' term does not contribute, but this term is only considered of marginal importance in Hubbard models.
[30] Y. Kamiya, N. Kawashima, and C. D. Batista, Phys. Rev. B **84**, 214429 (2011); A. L. Wysocki, K. D. Belashchenko, and V. P. Antropov, Nat. Phys. **7**, 485 (2011); M. Capati, M. Grilli, and J. Lorenzana, Phys. Rev. B **84**, 214520 (2011).
[31] S. Liang, A. Moreo, and E. Dagotto, Phys. Rev. Lett. **111**, 047004 (2013).
[32] General arguments[18] suggest that either $T_N = T_{Nem}$ in a first-order transition, or $T_N < T_{Nem}$ with both transitions being second order. Since we do not observe indications of metastabilities in the MC time evolution, or in histograms of observables, our results are compatible with the existence of a nematic regime.
[33] M. Daghofer, Q.-L. Luo, R. Yu, D. X. Yao, A. Moreo, and E. Dagotto, Phys. Rev. B **81**, 180514(R) (2010).
[34] At much larger temperatures $\sim U$ the PG disappears.
[35] S. Kumar and P. Majumdar, Eur. Phys. J. B **46**, 237 (2005).
[36] X. Zhang and E. Dagotto, Phys. Rev. **B 84** 132505 (2011).
[37] S. Liang, G. Alvarez, C. Sen, A. Moreo, and E. Dagotto, Phys. Rev. Lett. **109**, 047001 (2012).
[38] V. I. Anisimov, I. A. Nekrasov, D. E. Kondakov, T. M. Rice, and M. Sigrist, Eur. Phys. J. B **25**, 191 (2002); A. Georges, L. dé Medici, and J. Mravlje, Annu. Rev. Condens. Matter Phys. **4**, 137 (2013).
[39] M. Daghofer, A. Nicholson, A. Moreo, and E. Dagotto, Phys. Rev. B **81**, 014511 (2010).